Microelectronic Engineering 87 (2010) 1997–2001

Contents lists available at ScienceDirect

Microelectronic Engineering

journal homepage: www.elsevier.com/locate/mee

Frequency and temperature dependence of the dielectric and AC electrical conductivity in (Ni/Au)/AlGaN/AlN/GaN heterostructures

Engin Arslan [a,*], Yasemin Şafak [b], İlke Taşçıoğlu [b], Habibe Uslu [b], Ekmel Özbay [a]

[a] Nanotechnology Research Center, Department of Physics, Department of Electrical and Electronics Engineering, Bilkent University, Bilkent, 06800 Ankara, Turkey
[b] Department of Physics, Faculty of Arts and Sciences, Gazi University, 06500 Ankara, Turkey

ARTICLE INFO

Article history:
Received 28 September 2009
Received in revised form 4 December 2009
Accepted 16 December 2009
Available online 24 December 2009

Keywords:
(Ni/Au)/$Al_xGa_{1-x}N$/AlN/GaN heterostructures
Dielectric properties
AC electrical conductivity
Electric modulus
Passivation

ABSTRACT

The dielectric properties and AC electrical conductivity (σ_{ac})of the (Ni/Au)/$Al_{0.22}Ga_{0.78}N$/AlN/GaN heterostructures, with and without the SiN_x passivation, have been investigated by capacitance–voltage and conductance–voltage measurements in the wide frequency (5kHz–5 MHz) and temperature (80–400 K) range. The experimental values of the dielectric constant (ε'), dielectric loss (ε''), loss tangent ($\tan\delta$), σ_{ac} and the real and imaginary part of the electric modulus (M' and M'') were found to be a strong function of frequency and temperature. A decrease in the values of ε' and ε'' was observed, in which they both showed an increase in frequency and temperature. The values of M' and M'' increase with increasing frequency and temperature. The σ_{ac} increases with increasing frequency, while it decreases with increasing temperature. It can be concluded, therefore, that the interfacial polarization can occur more easily at low frequencies and temperatures with the number of interface states density located at the metal/semiconductor interface. It contributes to the ε' and σ_{ac}.

1. Introduction

The interface quality between the deposited metal and semiconductor surface is decisive for the performance and reliability of these devices. In general, the performance of metal-insulator/oxide-semiconductor (MIS or MOS) devices depends on various parameters, such as the interfacial passivation layer thickness and its homogeneity, distribution of the barrier height, density of the interface states at the metal and semiconductor interface, as well as the series resistance of a device, in which they must all be taken into account. Although silicon dioxide (SiO_2) is considered the traditional way to carry out an interfacial insulator/passivation layer in these devices, it cannot completely passivate the active dangling bonds at the semiconductor surface. Therefore, in recent years, dielectric materials, such as TiO_2 [1,2], HfO_2 [3], SiN_x [4–6], Al_2O_3 [7,8], ZrO_2 [9], $SrTiO_3$ [10] and $Bi_3Ti_4O_{12}$ [11,12] have been examined as potential materials for replacing SiO_2 in the MIS/MOS structures, MOS field effect transistor (MOSFET), metal-ferroelectric-insulator-semiconductor (MFIS) FET structures, and high electron mobility transistors (HEMTs) [13,14].

The interfacial passivation layer not only prevents the reaction and inter-diffusion between the metal and semiconductor substrate, but also alleviates the electric field reduction issue in these structures. When a bias voltage is applied across these structures, the combination of the interfacial passivation layer, depletion layer, and series resistance shares the applied voltage. In this respect, the interfacial passivation layer thickness, frequency, and temperature can influence the electrical and dielectric behavior of these structures [1,2,12,14–20].

Many studies have been conducted in recent years in order to investigate the effect of SiN_x passivation on the conduction mechanisms of two-dimension electron gas (2DEG) in $Al_xGa_{1-x}N$/GaN heterostructures [14–19]. Although the electrical properties of MIS, MOS, MOSFET, and HEMT structures have been studied for four decades, not much work has been carried out on the dielectric properties, especially considering the structures [18–20] in the wide frequency and temperature range. It is well known, in the ideal case, that the capacitance of MIS or MOS structures is usually frequency independent, especially at high frequencies ($f \geqslant 1$ MHz). However, the situation is different at low frequencies and temperatures. Depending on the frequency of the AC signal and temperature, there may be capacitance and conductance due to the interface states that are in excess of the depletion layer capacitance. The frequency and temperature responses of the dielectric ε', ε'', $\tan\delta$, σ_{ac} and electric modulus (M' and M'') are dominated by low frequency and temperature dispersion, whose physical origin has long been in question [18,20,21]. Therefore, it is very important to include the effects of frequency and temperature in the investigations of the electrical characteristics and dielectric properties in such devices.

* Corresponding author. Tel.: +90 312 2901020; fax: +90 312 2901015.
E-mail address: engina@bilkent.edu.tr (E. Arslan).

0167-9317/$ - see front matter © 2009 Elsevier B.V. All rights reserved.
doi:10.1016/j.mee.2009.12.067

In the present study, by using the capacitance–voltage (C–V) and conductance–voltage (G/ω–V) measurements, we investigated the frequency and temperature dependences of the electrical and dielectric parameters, such as ε', ε'', $\tan\delta$, σ_{ac} and the real and imaginary parts of the electric modulus (M' and M'') of (Ni/Au) Schottky contacts on unpassivated and SiN_x passivated $Al_{0.22}Ga_{0.78}N$/AlN/GaN heterostructures. In order to properly interpret these parameters, measurements were carried out in the wide frequency and temperature range of 5 kHz–5 MHz and 80–400 K, respectively.

2. Experimental details

The $Al_{0.22}Ga_{0.78}N$/AlN/GaN heterostructures were grown on c-plane (0 0 0 1) double-polished 2-inch diameter Al_2O_3 substrate in a low-pressure metalorganic chemical-vapor deposition reactor (MOCVD) (Aixtron 200/4 HT-S) by using trimethylgallium (TMGa), trimethylaluminum (TMAl), and ammonia as Ga, Al, and N precursors, respectively. Prior to the epitaxial growth, Al_2O_3 substrate was annealed at 1100 °C for 10 min in order to remove surface contamination. The buffer structures consisted of a 15 nm thick, low-temperature (650 °C) AlN nucleation layer along with high temperature (1150 °C) 420 nm AlN templates. A 1.5 μm nominally undoped GaN layer was grown on an AlN template layer at 1050 °C, which was followed by a 2 nm thick high temperature AlN (1150 °C) barrier layer. After the deposition of these layers, a 23 nm thick undoped $Al_{0.22}Ga_{0.78}N$ layer was grown on an AlN layer at 1050 °C. Finally, a 5-nm thick GaN cap layer growth was carried out at a temperature of 1085 °C and a pressure of 50 mbars.

The grown wafers were cut into several pieces and the ohmic and Schottky/rectifier contacts were made in the high vacuum coating system at approx. 10^{-7} Torr. The ohmic and Schottky contacts were formed as a square van der Pauw shape and as 1 mm diameter circular dots, respectively [13]. Prior to ohmic contact formation, the samples were cleaned with acetone in an ultrasonic bath. Then, a sample was treated with boiling isopropyl alcohol for 5 min and rinsed in de-ionized (DI) water that possessed 18 MΩ resistivity. After cleaning, the samples were dipped in a solution of HCl/H_2O (1:2) for 30 s in order to remove the surface oxides, and were then rinsed in DI water again for a prolonged period. Ti/Al/Ni/Au (16/180/50/150 nm) metals were thermally evaporated on the sample and were annealed at 850 °C for 30 s in N_2 ambient in order to form the ohmic contact.

After the formation of the ohmic contact, the SiN_x layer was deposited by plasma-enhanced chemical-vapor deposition (PECVD) on $Al_{0.22}Ga_{0.78}N$/AlN/GaN heterostructures surface at 300 °C. The SiN_x growth was optimized to have a low growth rate without changing the refractive index by a series of growth. After growth rate optimization, approximately 10 nm/min growth rates with a refraction index of 2.02 were achieved. And 4 and 10 nm thick SiN_x layers were deposited on sample B and C, respectively. The SiN_x thickness was measured exactly with ellipsometer. However, sample A was not passivated. Then Schottky contacts were formed by Ni/Au (50/80 nm) evaporation.

The capacitance–voltage (C–V) and conductance–voltage (G/ω–V) measurements were performed in the wide frequency range of 5 kHz–5 MHz by using an HP 4192A LF impedance analyzer (5 Hz–13 MHz), in which a small sinusoidal test signal of 40 mV peak to peak from the external pulse generator was applied to the sample as per the requirements. The temperature dependent measurements were performed in the wide temperature range of 80–400 K by using a Lake Shore model 321 auto-tuning temperature controllers with sensitivity better than ±0.1 K. All the measurements were carried out with the aid of a microcomputer through an IEEE-488 AC/DC converter card.

3. Results and discussion

3.1. Frequency dependent behavior of the dielectric properties and AC electrical conductivity

The frequency dependence of ε', ε', $\tan\delta$, σ_{ac} and the real and imaginary part of the electric modulus (M′ and M″) were evaluated from the knowledge of C–V and G/ω–V data for (Ni/Au)/$Al_{0.22}Ga_{0.78}N$/AlN/GaN heterostructures with SiN_x passivation layers (4 and 10 nm) and without passivation layer in the frequency range of 5 kHz–5 MHz, at room temperature. In order to describe the electric and dielectric properties of the structure, the complex permittivity can be defined in the following complex form [22,23],

$$\varepsilon^*(\omega) = \varepsilon' - j\varepsilon'' = \frac{C}{C_0} - j\frac{G}{\omega C_0} \tag{1}$$

where $\omega = 2\pi f$ is the angular frequency, ε' and ε'' are the real and imaginary part of complex permittivity, j is the imaginary root of -1 and C and G are the measured capacitance and conductance in the strong accumulation layer, respectively. Dielectric measurements, such as ε' and ε'' reveal significant information about the chemical and physical behavior of the electrical and dielectric properties. The values of the ε', at the various frequencies, can be calculated by using the measured capacitance values at the strong accumulation region from the relation [23–25],

$$\varepsilon' = \frac{C}{C_0} = \frac{Cd_p}{\varepsilon_0 A} \tag{2}$$

where C_0 is the capacitance of an empty capacitor, A is the rectifier contact area in cm^{-2}, d_p is the passivation layer thickness and ε_0 is dielectric constant of vacuum ($\varepsilon_0 = 8.85 \times 10^{-14}$ F/cm). In the strong accumulation region, the maximum capacitance of the structure corresponds to the insulator/passivation layer capacitance ($C_p = \varepsilon'\varepsilon_0 A/d_p$). The dielectric loss ($\varepsilon''$), at the various frequencies, can be calculated by using the measured conductance values from the relation,

$$\varepsilon'' = \frac{G}{\omega C_0} = \frac{Gd_p}{\varepsilon_0 \omega A} \tag{3}$$

The loss tangent ($\tan\delta$) can be expressed as follows [22–25],

$$\tan\delta = \frac{\varepsilon''}{\varepsilon'} \tag{4}$$

Fig. 1(a), inset of Fig. 1(a) and (b) shows the frequency dependent of the ε', ε'' and $\tan\delta$ plots of the (Ni/Au)/$Al_xGa_{1-x}N$/AlN/GaN heterostructures in the strong accumulation region, respectively, for the unpassivated (sample A) and SiN_x passivated samples (samples B and C). As shown in Fig. 1(a) and the inset of Fig. 1(a), the values of ε' and ε'' decrease with increasing frequency for three samples, while they remain nearly constant at sufficiently high frequencies ($f \geqslant 1$ MHz). These results nearly show the same trend for the ε' change with frequency for all the samples studied. On the other hand, the value of ε' increases with the increasing passivation layer thickness. Furthermore, it is clear that the values ε' and ε'' are greater at low frequencies due to the possible interface polarization mechanisms since interface states (N_{ss}) cannot follow the AC signal at high frequencies [2,11,12,26–29]. Interface polarization reaches a constant value due to the fact that beyond a certain frequency of the external field, the electron hopping cannot follow the alternative field. These dispersions in ε' and ε'' with frequency can be attributed to Maxwell–Wagner [26] and space-charge polarization [27]. As shown in Fig. 1(c), the values of $\tan\delta$ show a U shape behavior for sample A. However, the values of $\tan\delta$ for samples B and C increase with increasing frequency. Such behavior of $\tan\delta$ depends on many parameters, such as dislocation related N_{ss} that is localized between the metal and semiconductor,

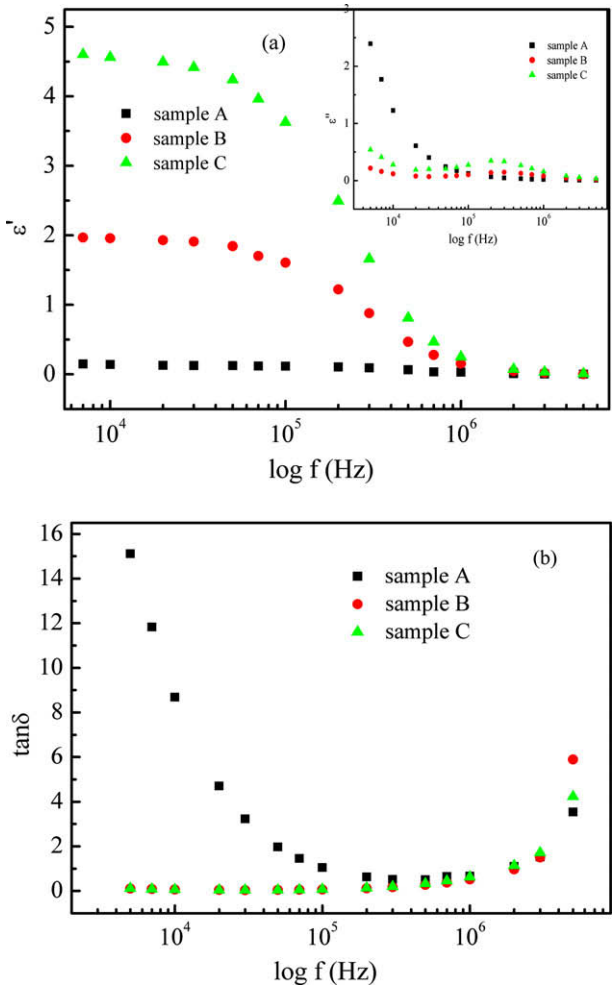

Fig. 1. The frequency dependences of (a) ε', ε'' (in the inset of Fig. 1(a)) and (b) tanδ and for (Ni/Au)/$Al_xGa_{1-x}N$/AlN/GaN heterostructures without (sample A) and with SiN_x passivation (sample B and C), respectively, at room temperature.

series resistance of devices (R_s), and thickness of the passivation layer. The experimental results show that the changes in frequency substantially alter the dielectric parameters of the (Ni/Au)/$Al_xGa_{1-x}N$/AlN/GaN heterostructure. In the case of the absence of an external electric field, the charge carriers that are bound at different localized states show different dipole orientations. An electron can hop between a pair of these centers under the applied an AC field, in turn leading to the reorientation of an electric dipole [26]. This process gives rise to a change in the dielectric constant. Therefore, the increase in the dielectric constant with decreasing frequency can be attributed to the effect of dipoles.

The AC electrical conductivity (σ_{ac}) of the dielectric material can be given by the following equation [23,27,28],

$$\sigma_{ac} = \omega C \tan\delta (d_p/A) = \varepsilon'' \omega \varepsilon_0 \quad (5)$$

Fig. 2 shows the variation of the AC conductivity (σ_{ac}) with frequency (in the frequency range 5 kHz–5 MHz) at room temperature. The electrical conductivity generally increases with increasing frequency and the thickness of the passivation layer [20,28].

The complex impedance (Z^*) and complex electric modulus (M^*) formalisms have been discussed by various authors with regard to the analysis of dielectric materials [29–32]. They prefer to describe the dielectric properties of these devices by using the electric modulus formalisms. The complex permittivity can be transformed into the M^* formalism by using the following relation [2,23,26–28]:

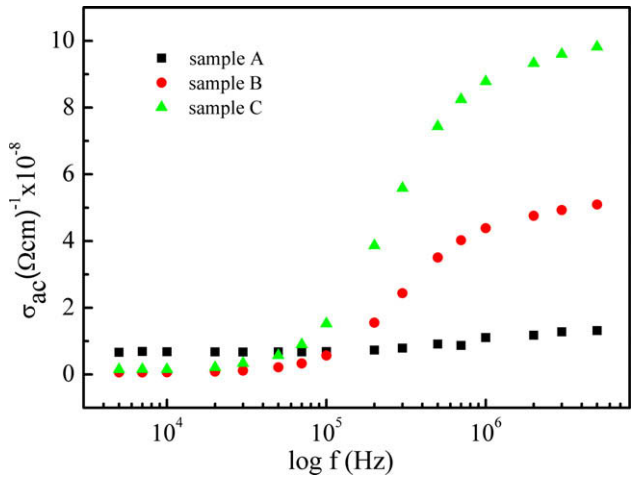

Fig. 2. The frequency dependences of the ac electrical conductivity (σ_{ac}) for (Ni/Au)/$Al_xGa_{1-x}N$/AlN/GaN heterostructures without (sample A) and with SiN_x passivation (sample B, and C), respectively, at room temperature.

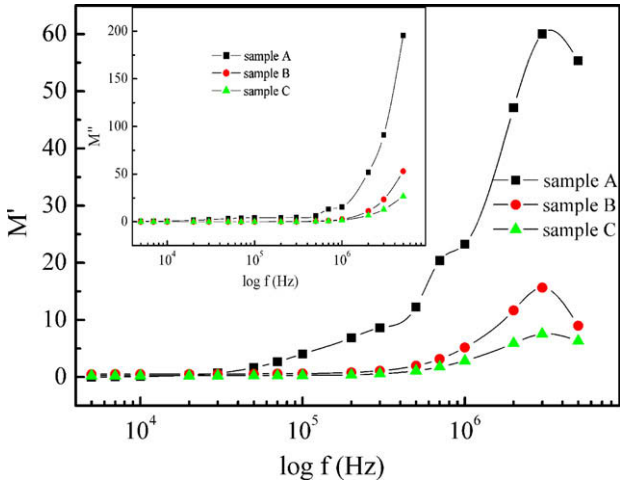

Fig. 3. Frequency dependence of the M' and M'' (in the inset of Fig. 3) for the unpassivated and SiN_x passivated (Ni/Au)/$Al_xGa_{1-x}N$/AlN/GaN heterostructure at room temperature (lines are given for eyes guide).

$$M^* = \frac{1}{\varepsilon^*} = M' + jM'' = \frac{\varepsilon'}{\varepsilon'^2 + \varepsilon''^2} + j\frac{\varepsilon''}{\varepsilon'^2 + \varepsilon''^2} \quad (6)$$

The real and imaginary parts of the electric modulus (M', M'') were determined by using ε' and ε'' values at room temperature, which are shown in Fig. 3 and the inset of Fig. 3, respectively, for all the samples. The variation of the real and imaginary parts of the electric modulus (M', M'') of the (Ni/Au)/$Al_xGa_{1-x}N$/AlN/GaN heterostructure as a function of frequency are shown in Fig. 3 and the inset of Fig. 3, respectively, at room temperature. It is evident from the inset of Fig. 3 that the values of M'' do not reach the maximum values even at the higher frequency of 5 MHz, which corresponds to $M_\infty = 1/\varepsilon_\infty$ due to the relaxation process. However, the M' reach a maximum value at approx. 3 MHz. Moreover, both of the values of M' and M'' nearly approach zero at low frequencies. These results are consistent with the reported results in the literature [27–30].

3.2. Temperature dependent behavior of the dielectric properties and AC electrical conductivity

The temperature dependence of the ε', ε'' and tanδ at 1 MHz for the (Ni/Au)/$Al_xGa_{1-x}N$/AlN/GaN heterostructure is shown in

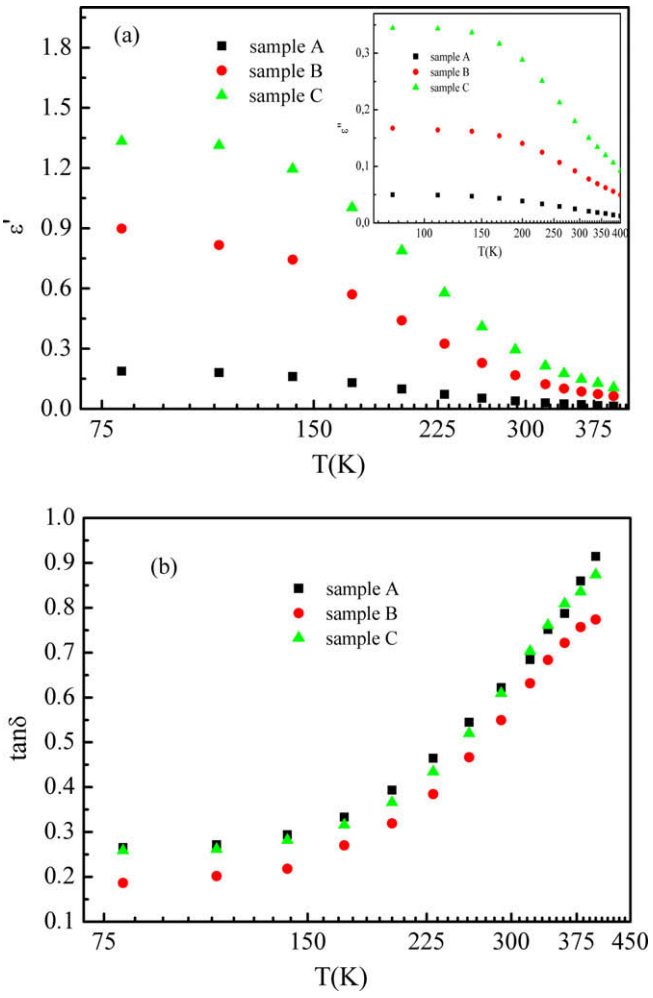

Fig. 4. The temperature dependence of the (a) ε', ε'' (in the inset of Fig. 4(a)) and (b) tanδ at 1 MHz for the unpassivated and SiN_x passivated (Ni/Au)/$Al_xGa_{1-x}N$/AlN/GaN heterostructure.

Fig. 4(a), inset of Fig. 4(a), and Fig. 4(b), respectively. As can be seen in Fig. 4(a) and the inset of Fig. 4(a), both ε' and ε'' decrease with increasing temperature, which is similar to the effect of frequency (Fig. 1(a) and the inset of that figure). These results show that the magnitude of the disorders decreases with increasing temperature. The frequency and temperature dependence of ε' and ε'' are small at high frequencies and temperatures. In addition, the values of ε' and ε'' increase with increasing passivation layer thickness, especially at low frequencies and temperatures. Contrary to ε' and ε'', the value of tanδ increases as the temperature is increased.

Fig. 5 and the inset of Fig. 5 show the real part of M' and the imaginary part of M'' of the electric modulus M^* versus the temperature for the studied samples at 1 MHz. It can be clearly seen in Fig. 5, and the inset of that figure, that the M' and M'' increase with increasing temperature for all the samples. These behaviors are attributed to the polarization increase with increasing temperature in the (Ni/Au)/$Al_{0.22}Ga_{0.78}N$/AlN/GaN heterostructures.

Fig. 6(a) shows the temperature dependence of the AC electrical conductivity in the (Ni/Au)/$Al_xGa_{1-x}N$/AlN/GaN heterostructure at 1 MHz for all the samples. It is clear that the conductivity decreases with the increasing measured temperature range for all samples. These behaviors of conductivity result from decreasing conductance with increasing temperature. The relationship between the AC electrical conductivity and the absolute temperature can be written as:

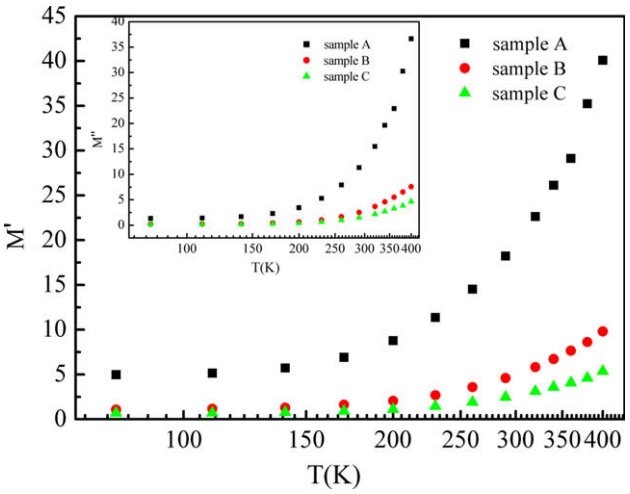

Fig. 5. Temperature dependence of the M' and M'' (in the inset of Fig. 5) for the unpassivated and SiN_x passivated (Ni/Au)/$Al_xGa_{1-x}N$/AlN/GaN heterostructure at room temperature.

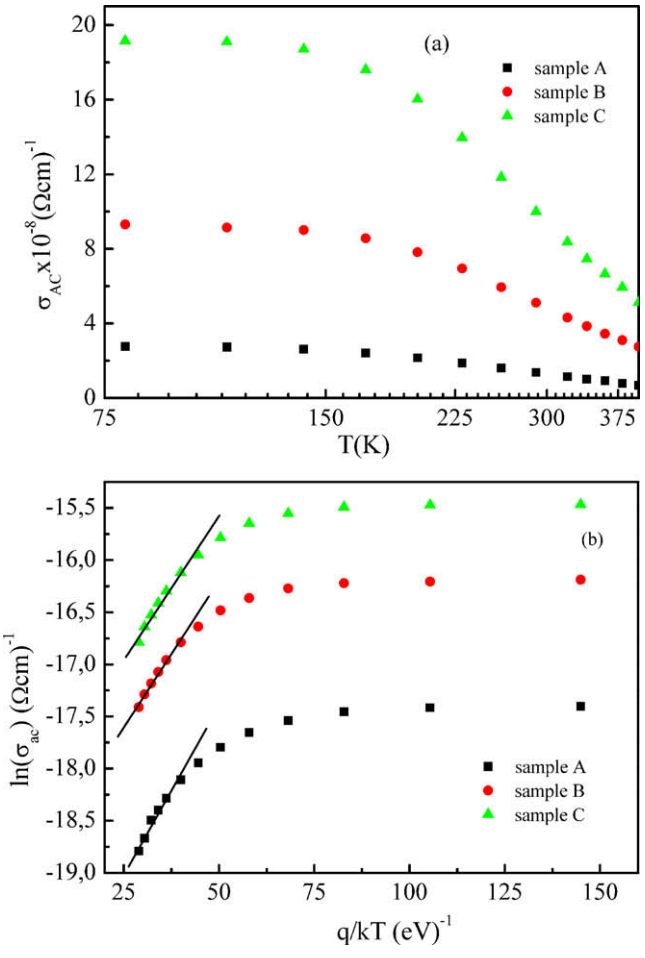

Fig. 6. (a) The behavior of the electrical conductivity (σ_{ac}) as a function of temperature. (b) The variation of the $ln\sigma_{ac}$ vs. q/kT characteristics of the unpassivated and SiN_x passivated (Ni/Au)/$Al_xGa_{1-x}N$/AlN/GaN heterostructures at 1 MHz. The lines in Fig. 6(b) show the linear fit function.

$$\sigma = \sigma_0 \exp\left(\frac{-E_a}{kT}\right) \tag{7}$$

where σ_0 represents the composite constant, k the Boltzmann constant, and E_a is the activation energy. Additionally, the values of σ_{ac} increase with the increasing passivation layer thickness, especially at low temperatures.

Fig. 6(b) shows the Arrhenius plot of the AC electrical conductivity data obtained in the temperature range of 80–400 K. As can be seen in Fig. 6(b), the $ln\sigma_{ac}$ vs. q/kT plot at 1 MHz shows linear behavior in the temperature range of 260–400 K. However, at low temperatures these plots deviate from the linearity. Such behavior of σ_{ac} implies that the E_a is dependent upon temperature, in which two different conduction mechanisms may dominate in this temperature range. The slope of the $ln\sigma_{ac}$ vs. q/kT plot can be positive or negative according to the conductive behavior of the materials. In the present study, the values of conductance decreased with the increasing temperature for all the samples. Therefore, the $ln\sigma_{ac}$ vs. q/kT plots shows a positive slope. Such behavior generally can be observed in high dielectric materials, such as $SrTa_2O_6$, HfO_2 and ZrO_2 [31]. In Fig. 6(b), the high temperature ranges from 260–400 K, in which the data of the samples can be fitted in a straight line, in turn representing the activation energy of 45.7, 42.9, and 45.8 meV for samples A, B, and C, respectively. This low activation energy value is associated with recombination, which causes even more departures from the thermionic-emission behavior at low temperatures [20]. The conduction electrons may be created from the donor state as a possible consequence of ionized oxygen vacancies. At high temperatures, these carriers are released and recombined [32]. Therefore, conduction at high temperatures is found to be merged.

4. Conclusions

The dielectric properties and AC electrical conductivity (σ_{ac}) of the (Ni/Au) Schottky contacts on $Al_xGa_{1-x}N$/AlN/GaN heterostructures, with the SiN_x passivation layers (4 and 10 nm) and without a passivation layer, have been investigated by the C–V and G/ω–V measurements in the wide frequency and temperature range of 5 kHz–5 MHz and 80–400 K, respectively. The experimental results show that the values of ε' and ε'' are found to decrease with increasing frequency and temperature. The values of σ_{ac} increase with increasing frequency and the passivation layer thickness, while they decrease with increasing temperature. The values of M' and M'' increase with both increasing frequency and temperature. The interfacial polarization can occur more easily at low frequencies and temperatures, in which the number of interface states density at the metal/SiN_x interface, consequently contributes to the improvement of the dielectric properties of heterostructures. The C–V and G/ω–V characteristics confirmed that both frequency and temperature strongly affect the dielectric properties and AC electrical conductivity.

Acknowledgments

This work is supported by the European Union under the projects EU-PHOME, and EU-ECONAM, and TUBITAK under Project Nos. 107A004 and 107A012. One of the authors (E.O.) also acknowledges partial support from the Turkish Academy of Sciences.

References

[1] H.K. Ha, M. Yoshimoto, B.K. Moon, H. Ishiwara, Appl. Phys. Lett. 66 (1996) 2965.
[2] O. Pakma, N. Serin, T. Serin, Ş. Altındal, J. Phys. D: Appl. Phys. 41 (2008) 215103.
[3] F.C. Chiu, W.C. Shih, J.Y.M. Lee, H.L. Hwang, Microelectron. Reliab. 47 (2007) 548.
[4] B.R. Chakraborty, N. Dilawar, S. Pal, D.N. Bose, Thin Solid Films 411 (2002) 240.
[5] M.M. Bülbül, S. Zeyrek, Ş. Altındal, H. Yüzer, M.M. Bülbül, Microelectron. Eng. 83 (2006) 577.
[6] Marcin Miczek, Chihoko Mizue, Tamotsu Hashizume, Bogusława Adamowicz, J. Appl. Phys. 103 (2008) 104510.
[7] T. Hashizume, S. Ootomo, H. Hasegawa, Phys. Status Solidi (c) 0 (2003) 2380.
[8] Q. Feng, Y. Hao, Y.-Z. Yue, Semicond. Sci. Technol. 24 (2009) 025030.
[9] M.K. Bera, S. Chakraborty, S. Saha, D. Paramanik, S. Varma, S. Bhattacharya, C.K. Maiti, Thin Solid Films 504 (2006) 183.
[10] M.J. Hua, M.X. Jian, L. Tie, L.S. Jian, Z.X. Dong, S.J. Lan, C.J. Hao, Chin. Phys. 14 (2005) 2352.
[11] F. Parlaktürk, Ş. Altındal, A. Tataroğlu, M. Parlak, A. Agasiyev, Microelectron. Eng. 85 (2008) 81.
[12] B.H. Park, S.J. Hyun, C.R. Moon, B.-D. Choe, J. Lee, C.Y. Kim, W. Jo, T.W. Noh, J. Appl. Phys. 84 (1998) 4428.
[13] Engin Arslan, Semsettin Altındal, Suleyman Ozcelik, Ekmel Ozbay, J. Appl. Phys. 105 (2009) 023705.
[14] W. Huang, T. Khan, T.P. Chow, J. Electron. Mater. 35 (2006) 726.
[15] Z.H. Feng, Y.G. Zhou, S.J. Cai, K.M. Lau, Appl. Phys. Lett. 85 (2004) 5248.
[16] J. Derluyn, S. Boeykens, K. Cheng, R. Vandersmissen, J. Das, W. Ruythooren, S. Degroote, M.R. Leys, M. Gremain, G. Borghs, J. Appl. Phys. 98 (2005) 054501.
[17] M.J. Wang, B. Shen, F.J. Xu, Y. Wang, J. Xu, S. Huang, Z.J. Yang, Z.X. Qin, G.Y. Zhang, Phys. Lett. A 369 (2007) 249.
[18] M.M. Bülbül, Microelectron. Eng. 84 (2007) 124.
[19] L. Aballe, L. Gregoratti, A. Barinov, M. Kiskinova, T. Clausen, S. Gangopadhyay, J. Falta, Appl. Phys. Lett. 84 (2004) 5031.
[20] A. Tataroğlu, Ş. Altındal, M.M. Bülbül, Microelectron. Eng. 81 (2005) 140.
[21] S. Kar, S. Varma, J. Appl. Phys. 58 (1985) 4256.
[22] Vera V. Daniel, Dielectric Relaxation, Academic Press, London, 1967.
[23] P. Pissis, A. Kyritsis, Solid State Ionics 97 (1997) 105.
[24] M. Popescu, I. Bunget, Phys. Solid Dielectrics, Elsevier, Amsterdam, 1984.
[25] A. Chelkowski, Dielectric Physics, Elsevier, Amsterdam, 1980.
[26] O. Bidault, P. Goux, M. Kchikech, M. Belkaoumi, M. Maglione, Phys. Rev. B 49 (1994) 7868.
[27] C. Fanggao, G.A. Saunders, E.F. Lambson, R.N. Hampton, G. Carini, G.D. Marco, M. Lanza, J. Polym. Sci. Part B: Polym. Phys. 34 (1996) 425.
[28] K. Prabakar, S.K. Narayandass, D. Mangalaraj, Phys. Status Solidi A 199 (2003) 507.
[29] A.A. Sattar, S.A. Rahman, Phys. Status Solidi A 200 (2003) 415.
[30] İ.M. Afandiyeva, İ. Dökme, Ş. Altındal, M.M. Bülbül, A. Tataroğlu, Microelectron. Eng. 85 (2008) 247.
[31] E.H. Rhoderick, R.H. Williams, Metal-Semiconductor Contacts, second ed., Clarendon Press, Oxford, 1988.
[32] R.N.P. Choudhary, D.K. Pradhan, C.M. Tirado, G.E. Bonilla, R.S. Katiyar, Physica B 393 (2007) 24.